Silicon photonic crystal nanostructures for refractive index sensing

Dorfner, Dominic; Hürlimann, T.; Zabel, T.; Frandsen, Lars Hagedorn; Abstreiter, G.; Finley, J.J.

Published in:
Applied Physics Letters

Link to article, DOI:
10.1063/1.3009203

Publication date:
2008

Document Version
Publisher's PDF, also known as Version of record

Silicon photonic crystal nanostructures for refractive index sensing

D. F. Dorfner,[1,a)] T. Hürlimann,[1] T. Zabel,[1] L. H. Frandsen,[2] G. Abstreiter,[1] and J. J. Finley[1,b)]

[1]*Walter Schottky Institut and Physik Department, Technische Universität München, Am Coulombwall 3, D-85748 Garching, Germany*

[2]*DTU Fotonik, Department of Photonics Engineering, Technical University of Denmark, DK-2800 Kgs. Lyngby, Denmark*

(Received 22 July 2008; accepted 7 October 2008; published online 3 November 2008)

The authors present the fabrication and optical investigation of silicon on insulator photonic crystal drop filters for use as refractive index sensors. Two types of defect nanocavities ($L3$ and $H1-r$) are embedded between two W1 photonic crystal waveguides to evanescently route light at the cavity mode frequency between input and output waveguides. Optical characterization of the structures in air and various liquids demonstrates detectivities in excess of $\Delta n/n=0.018$ and $\Delta n/n=0.006$ for the $H1-r$ and $L3$ cavities, respectively. The measured cavity frequencies and detector refractive index responsivities are in good agreement with simulations, demonstrating that the method provides a background free transducer signal with frequency selective addressing of a specific area of the sensor chip. © *2008 American Institute of Physics*. [DOI: 10.1063/1.3009203]

Silicon photonic crystals (PhCs) have received great attention over recent years due to the strong potential they provide for applications in the fields of integrated optics[1,2] and optical sensing.[3–5] Nanoscale optical cavities formed by introducing point defects into two dimensional PhCs are particularly interesting since they typically support highly localized cavity modes. The wavelength (λ_m) and quality factor ($Q=\lambda_m/\Delta\lambda$) of these modes are sensitive to the local refractive index (RI) of the environment, providing a transducer signal for constructing nanoscale optical sensors. Existing approaches for RI sensing typically utilize surface plasmon resonance (SPR) (Ref. 6) or interferometric methods[7] to provide extremely high sensitivities in the range $\Delta n/n=10^{-7}-10^{-8}$ with detector areas of the order of ~ 1 mm^2. By contrast, PhC nanocavity sensors tend to have lower sensitivities ($\Delta n/n=10^{-2}-10^{-4}$) but can be designed to fully localize the optical field to an area of ~ 1 μm^2, corresponding to only ~ 1 fl of analyte. Furthermore, many PhC sensors can be readily integrated onto a chip and integrated with optical routing components.

Various groups have reported sensing based on PhC nanostructures. A detection limit of $\Delta n/n=0.0056$ was demonstrated by Loncar *et al.*[8] using GaAs nanocavity lasers. Other groups used evanescent coupling from ridge waveguides (WGs) to a silicon PhC nanocavity in a serial geometry, achieving sensitivities of $\Delta n/n=0.002$.[9,10] Sensors based on measuring the transmission properties of PhC-WGs were investigated by Erickson *et al.*[11] and Skivesen *et al.*[12] Cunningham *et al.*[13] utilized an alternative approach based on detecting the RI from a two-dimensional Bragg grating. However, as for SPR and interferometric methods this approach is nonlocal and requires a large analyte volume.

Unlike previously reported PhC sensors that rely on direct coupling from a WG to the PhC cavity,[8–10,12] we employ a drop filter consisting of a resonant cavity *between* two spatially separated PhC-WGs. This allows many detectors to be selectively addressed in parallel via the resonant frequency and readily lends itself to operation in a liquid flow cell. After describing our sample design and fabrication technology, we present the experimental results and compare our findings with simulations. Two types of cavity designs are compared: $L3$ cavities[14] (three missing holes) and $H1-r$ defects[15] (tuned radius of a single hole) in air and when the structures are infiltrated with various solutions. The results reveal sensitivities of $\Delta n/n=0.018$ for the $H1-r$ design and $\Delta n/n=0.006$ for the $L3$ cavity, illustrating an integrated approach for RI sensing based on silicon PhC nanocavities.

We fabricated PhC nanocavities from the silicon-on-insulator material system with a top Si layer of thickness 300 nm on a 1 μm thick buried oxide layer. A JEOL-JBX9300FS electron beam lithography system was used to define high-resolution structures into the electron beam resist, which was subsequently used as a soft etching mask to form the PhC nanostructure. The structures investigated consist of a hexagonal lattice (pitch a) of air holes perforating the top Si layer into which cavities are formed by introducing point defects into the lattice. This pattern was transferred through the Si layer using an inductively coupled plasma reactive ion etching system to define air cylinders with vertical sidewalls. In the final step, freestanding silicon membranes were formed by selectively removing the buried SiO_2 layer using hydrofluoric acid. In Fig. 1 we show a scanning electron microscopy (SEM) image of one of the investigated structures. A tapered ridge WG is used to guide the light over a distance of ~ 2 mm from the sample cleaved facet into a W1 PhC-WG. The nanocavities are defined in the periodic crystal immediately adjacent to the WG and separated by two to three lattice periods from it. This enables efficient evanescent coupling of light from the PhC-WG into the cavity. The cavities form the active sensing area of our device.[16]

Figure 1 (left) shows a representative image obtained using high resolution SEM measurements of a fabricated PhC nanocavity coupled to the W1 WG. When introducing a line defect by removing lattice points along one direction, WG modes within the photonic band gap (PBG) arise. The even WG modes are highlighted in Fig. 1 (right-panel) as the

a)Electronic mail: dorfner@wsi.tum.de.
b)URL: www.wsi.tum.de.

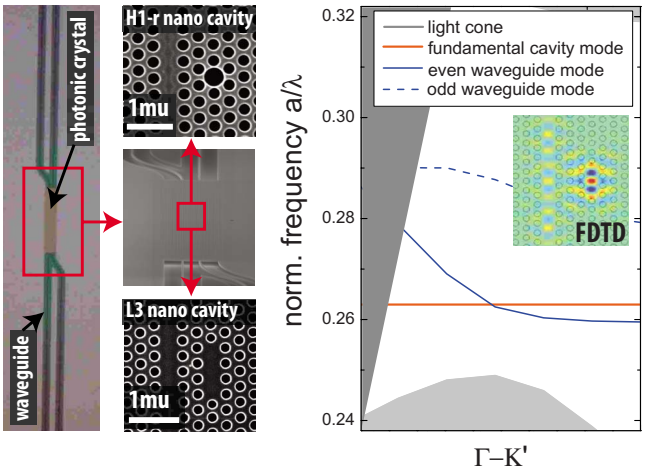

FIG. 1. (Color online) (left) SEM images showing the $H1-r$ and $L3$ defects in vicinity of the PhC-WG. (right) Photonic band diagram showing the dispersion of the W1-PhC-WG in reciprocal space (blue) and the fundamental cavity mode of an $L3$ defect (red). The inset depicts the E_y-field distribution obtained by FDTD simulation for optical excitation into the WG resonant with the cavity mode frequency.

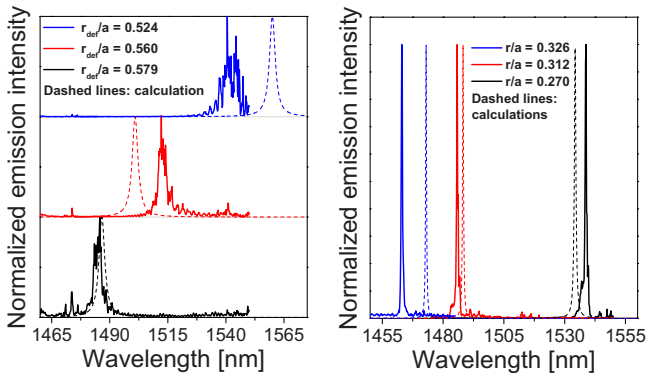

FIG. 2. (Color online) (left) Cavity mode of $H1-r$ designs with fixed $r/a=0.27$ and various defect radii r_{def}/a compared with calculations depicted as dashed lines. (right) Cavity mode of $L3$ designs with various hole radii r/a compared with calculations.

continuous blue line on the figure. Also presented is the photonic band diagram of a PhC W1-WG in the normalized unit a/λ ($r/a=0.3$, $h/a=0.7$ along the $\Gamma-K'$ (nearest-neighbor) direction obtained by plane wave expansion simulations. The WG mode lies within the frequency range of $0.26 \leq a/\lambda \leq 0.28$. The PBG denoted by the white shaded background spans the range from $a/\lambda \sim 0.25-0.32$. The red horizontal line at $a/\lambda=0.265$ represents the lowest localized cavity mode of an $L3$ cavity. At $k \sim 0.3(\pi/a)$ the WG and cavity modes intersect, enabling efficient coupling of the guided light in the WG to the cavity.

In order to investigate the optical properties of the PhC nanocavities, we used an experimental setup described in the following. Linear polarized light from a tunable external cavity diode laser is coupled into a single mode fiber and connected to a piezo controlled lensed fiber with a working distance of 14 μm from the sample facet. Before reaching the sample, the polarization is carefully set to be TE-like. This is essential since the band structure presented in Fig. 1 reflects even, TE-like modes. The signal is then collected using a piezo controlled 100× microscope objective in normal orientation to the structure surface, enabling a spatial resolution at the diffraction limit. We use a sensitive infrared camera (Vidicon PbO-PbS-IR) to verify the local emission at the cavity site by imaging the sample surface and detect the incoupled power into the cavity mode in vertical direction using a single mode fiber in confocal geometry focused on the cavity. In order to investigate the cavity modes in aqueous environments, we introduced a flow cell with a glass cover plate that enables measurements while various solutions are introduced to the PhC.

The cavity mode frequency depends strongly on both the geometric parameters of the structure and the local RI in the vicinity of the cavity. The cavity mode shifts to higher frequencies when increasing r/a and, in the case of the $H1-r$ cavities, it can be additionally tuned by varying the defect radius r_{def}/a. We systematically fabricated a wide range of PhC nanocavities with various designs and thoroughly investigated their resonant wavelength and mode finesse. Special care was taken to design structures with overlapping WG and cavity modes to allow efficient in coupling from the WG into the nanocavity. In Fig. 2 we show the vertical emission spectrum from typical $H1-r$ (left) and $L3$ (right) cavities with different geometries. The solid lines on the figure show the experimental measurements and the dashed lines represent calculations of the cavity mode wavelength and Q-factor. Defect radii $r_{\mathrm{def}}/a(1)=0.524$, $r_{\mathrm{def}}/a(2)=0.560$, and $r_{\mathrm{def}}/a(3)=0.579$ give rise to measured cavity modes at $\lambda_1=1541.8$ nm ($Q_1=197$), $\lambda_2=1512.6$ nm ($Q_2=413$), and $\lambda_3=1485.1$ nm ($Q_3=438$), respectively, for $r/a=0.27$ and $a=380$ nm. The measured values are in very good agreement with the calculated values $\lambda_{1c}=1560.0$ nm, $\lambda_{2c}=1500.9$ nm, and $\lambda_{3c}=1486.6$ nm obtained by plane wave expansion method. The slight offset of a few nanometers between measurement and calculation is due to the uncertainty of determining the defect radius r_{def}/a using a plain view SEM and the finite spatial discretization grid used for the calculations. Furthermore, the measured mode Q-factors ($Q \sim 400$) are of the order of the calculated value $Q \sim 600$ (obtained by FDTD) for the $H1-r$ cavities. The Q-factor is mainly limited by in-plane losses into the PhC-WG and vertical radiation.

In order to obtain higher Q-factors and higher sensitivities, we also fabricated $L3$ cavities formed by three missing holes in the PhC lattice with typical Q-factors around ~2700. Figure 2 (right) shows the typical vertical emission spectra of a number of $L3$ cavities with increasing r/a ratio and $a=380$ nm. A clear shift to higher wavelengths is observed as r/a decreases. The measured resonant modes and their Q-factor agree very well with the calculated values as summarized together with the results of the $H1-r$ cavity in Table I.

TABLE I. Measured and calculated values of the $H1-r$ and $L3$ cavities as a function of the r_{def}/a and r/a ratio.

Cavity	r_{def}/a, r/a	λ_{mes} (nm)	λ_{calc} (nm)	Q_{mes}	Q_{calc}
$H1-r$	0.524	1541.8	1560.0	197	915
$H1-r$	0.560	1512.6	1500.9	413	634
$H1-r$	0.579	1485.1	1486.6	438	512
$L3$	0.270	1463.1	1473.0	2686	3436
$L3$	0.312	1485.8	1488.2	2742	3160
$L3$	0.326	1538.7	1534.3	2732	1988

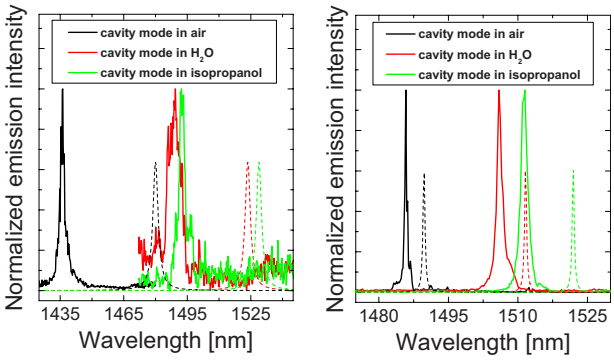

FIG. 3. (Color online) Cavity mode measured in air ($n=1.00$), water ($n=1.33$), and IPA ($n=1.377$) for a $H1-r$ cavity (left panel) and an $L3$ cavity (right panel).

The resonant wavelengths match the calculated values within an accuracy better than ~10 nm for the $L3$ cavity. Moreover, the measured Q-factor is comparable to the calculated value of the structure, indicating that it is limited by radiation losses into the W1 WG and not by fabrication imperfections.

We now continue to discuss the dependence of the cavity mode wavelength on the RI. We used three liquids to infiltrate the PhC: air ($n=1.0$), water ($n=1.33$), and isopropanol (IPA) ($n=1.377$). By increasing the RI in the holes of the PhC, the PBG shrinks and the cavity modes shift to lower frequencies.

In Fig. 3 we present the recorded spectra in these three liquids of a specific $H1-r$ cavity (left) with the geometric parameters $a=380$ nm, $r/a=0.325$, $h/a=0.8$, and $r_{\mathrm{def}}/a=0.5$ and an $L3$ cavity (right) with geometric parameters $a=380$ nm, $r/a=0.312$, and $h/a=0.8$. The measurements in air, water, and IPA are denoted by the black, red, and green curves, respectively. The resonant wavelength of the $H1-r$ cavity changes from $\lambda_{\mathrm{air}}=1436.0$ nm ($Q_{\mathrm{air}}=591$) to $\lambda_{\mathrm{H_2O}}=1488.8$ nm ($Q_{\mathrm{H_2O}}=246$) and $\lambda_{\mathrm{IPA}}=1492.5$ nm ($Q_{\mathrm{IPA}}=460$). The dashed lines show the simulated mode wavelength for the different RIs: $\lambda_{S-\mathrm{air}}=1480.0$ nm, $\lambda_{S-\mathrm{H_2O}}=1523.6$ nm, and $\lambda_{S-\mathrm{IPA}}=1528.9$ nm. The experimental data follow the expected trend rather well, albeit with an offset of $\Delta\lambda\sim40$ nm. We ascribe this shift mainly to the uncertainty in accurately determining the geometric parameters of the PhC structure correctly and the finite spatial grid used in the calculations. With a slightly increased size of the defect hole of $r_{\mathrm{def}}/a=0.525$ instead of $r_{\mathrm{def}}/a=0.5$, we obtain $\lambda_{S-\mathrm{air}}=1480.0$ nm, $\lambda_{S-\mathrm{H_2O}}=1513.5$ nm, and $\lambda_{S-\mathrm{IPA}}=1519.1$ nm in good agreement with the measurements.

The resonant wavelength of the $L3$ cavity changes from $\lambda_{\mathrm{air}}=1486.5$ nm ($Q_{\mathrm{air}}=2742$) to $\lambda_{\mathrm{H_2O}}=1504.8$ nm ($Q_{\mathrm{H_2O}}=958$) and $\lambda_{\mathrm{IPA}}=1511.7$ nm ($Q_{\mathrm{IPA}}=1096$). Again the simulated values are depicted by dashed lines in Fig. 3 with the following values: $\lambda_{S-\mathrm{air}}=1489.7$ nm, $\lambda_{S-\mathrm{H_2O}}=1511.7$ nm, and $\lambda_{S-\mathrm{IPA}}=1521.9$ nm. The agreement between experimental data and calculation is satisfactory and the results are quantitatively compared in Table II.

These measurements allow us to calculate a sensitivity of the signal on the ambient RI. For the $H1-r$ cavities we obtain a slope of $\Delta\lambda/\Delta n=155\pm6$. Assuming a typical $Q\sim400$ and a minimal detectable shift of $\Delta\lambda\sim1500$ nm/$400\sim3.75$ nm, we obtain a detection limit of $\Delta n/n\sim0.018$. For the $L3$ cavities we obtain a slope of $\Delta\lambda/\Delta n=63\pm9$, that for $Q\sim3000$, and a limited shift of $\Delta\lambda\sim1500$ nm/$3000\sim0.5$ nm leads to a detection limit of $\Delta n/n\sim0.006$. Table II compares the theoretical and measured sensitivities $\Delta n/n$ for both defect designs $L3$ and $H1-r$.

TABLE II. Measured and calculated cavity mode wavelengths as a function of different background RIs. The last row compares the detection limit achieved with the two defect designs assuming a detection limit of one mode linewidth.

	$H1-r_{\mathrm{measured}}$	$H1-r_{\mathrm{calc}}$	$L3_{\mathrm{measured}}$	$L3_{\mathrm{calc}}$
λ_{air} (nm)	1436.0	1480.0	1486.5	1489.73
$\lambda_{\mathrm{H_2O}}$ (nm)	1488.8	1523.6	1504.8	1511.7
λ_{iso} (nm)	1492.5	1528.9	1511.7	1521.9
$\Delta n/n$	0.018	0.014	0.006	0.004

In summary, we presented a RI-sensor based on a PhC drop filter. Two nanocavity designs were investigated: the $H1-r$ and the $L3$ cavities, both of which were probed in air and our findings were shown to be in very good agreement with FDTD simulations. Experimental data confirming the sensing principle of our device were presented by introducing fluids with different RIs as a background material: air, water, and IPA. An extrapolated detection limit of $\Delta n/n=0.018$ was demonstrated for the $H1-r$ design and $\Delta n/n=0.006$ for the $L3$ nanocavities. Our results confirm the suitability of the devices fabricated for highly local RI sensing based on silicon PhC nanostructures. The detection limit could be further improved by increasing the cavity Q (Ref. 16) or by optimizing the cavity design to push the optical mode into the low RI region.[17]

Financial support of the German Excellence Initiative via the "Nanosystems Initiative Munich (NIM)," the CompInt program of the Elite Network of Bavaria, and from the Danish Technical Research Council via the CORAL (coupled PhC resonator array lasers) project is gratefully acknowledged.

[1] T. Krauss and R. Rue, Prog. Quantum Electron. **23**, 51 (1999).
[2] L. Thylen, M. Qui, and S. Anand, ChemPhysChem **5**, 1268 (2004).
[3] I. White and X. Fan, Opt. Express **16**, 1020 (2008).
[4] N. Mortensen, S. Xiao, and J. Pedersen, Microfluid. Nanofluid. **4**, 117 (2008).
[5] D. Dorfner, T. Hürlimann, G. Abstreiter, and J. Finley, Appl. Phys. Lett. **91**, 233111 (2007).
[6] J. Homola, S. Yee, and G. Gauglitz, Sens. Actuators B **54**, 3 (1999).
[7] R. Heideman and P. Lambeck, Sens. Actuators B **61**, 100 (1999).
[8] M. Loncar, A. Scherer, and Y. Qiu, Appl. Phys. Lett. **82**, 4648 (2003).
[9] E. Chow, A. Grot, L. Mirkarimi, M. Sigalas, and G. Girolami, Opt. Lett. **29**, 1093 (2004).
[10] M. Lee and P. Fauchet, Opt. Express **15**, 4530 (2007).
[11] D. Erickson, T. Rockwood, T. Emery, A. Scherer, and D. Psaltis, Opt. Lett. **31**, 59 (2006).
[12] N. Skivesen, A. Tetu, M. Kristensen, J. Kjems, L. Frandsen, and P. Borel, Opt. Express **15**, 3169 (2007).
[13] B. Cunningham, P. Le, B. Lin, and J. Papper, Sens. Actuators B **81**, 316 (2002).
[14] Y. Akahane, T. Asano, B. Song, and S. Noda, Nature (London) **425**, 944 (2003).
[15] S. Noda, A. Chutinan, and M. Imada, Nature (London) **407**, 608 (2000).
[16] B. Song, S. Noda, T. Asano, and Y. Akahane, Nature Mater. **4**, 207 (2005).
[17] S. Kwon, T. Suenner, M. Kamp, and A. Forchel, Opt. Express **16**, 11709 (2008).